ISA Transactions ■ (■■■■) ■■■–■■■

Contents lists available at ScienceDirect

ISA Transactions

journal homepage: www.elsevier.com/locate/isatrans

Fast Fourier and discrete wavelet transforms applied to sensorless vector control induction motor for rotor bar faults diagnosis

Hicham Talhaoui [a,b,*], Arezki Menacer [a], Abdelhalim Kessal [b], Ridha Kechida [a,c]

[a] LGEB Laboratory, University of Biskra, Algeria
[b] University of Bordj Bou Arreridj, Algeria
[c] University of El-Oued, Algeria

ARTICLE INFO

Article history:
Received 12 March 2014
Received in revised form
1 June 2014
Accepted 9 June 2014
This paper was recommended
for publication by Jeff Pieper

Keywords:
Induction motor
Fault diagnosis
Broken rotor bars
Discrete wavelet analysis
Fast Fourier transforms
Sensorless
Luenberger observer
Sensoless vector control

ABSTRACT

This paper presents new techniques to evaluate faults in case of broken rotor bars of induction motors. Procedures are applied with closed-loop control. Electrical and mechanical variables are treated using fast Fourier transform (FFT), and discrete wavelet transform (DWT) at start-up and steady state. The wavelet transform has proven to be an excellent mathematical tool for the detection of the faults particularly broken rotor bars type. As a performance, DWT can provide a local representation of the non-stationary current signals for the healthy machine and with fault. For sensorless control, a Luenberger observer is applied; the estimation rotor speed is analyzed; the effect of the faults in the speed pulsation is compensated; a quadratic current appears and used for fault detection.

1. Introduction

Electrical motors are extensively used in industrial applications requiring high performances, where motor speed should closely follow a specified reference trajectory regardless of any load disturbance, parameters variations and model uncertainties. In order to achieve high performance, the field-oriented control of the induction motor drive is employed. However, the control design of such system plays a role in system performance improvement. The decoupling characteristics of vector control induction motor affect adversely the parameters changes in the motor [1]. However, they are subject to failures due to production processes or operating conditions [2]. The rotor failures are caused by a combination of various stresses that act in the rotor, which can be electromagnetic, thermal, residual, dynamic, environmental and mechanical [3].

The diagnosis of induction motor faults in line-connected motors has been extensively investigated in the last decade, and several diagnostic procedures have been proposed with this aim. However, it is recognized that the techniques developed in line-fed induction motors, and open loop drives cannot be used straightforward when the motor is included in a more complex control structure based on direct torque control and field oriented control [4]. For closed-loop drives, the control loops mask the fault effect. Some attempts can be found in literature about using d (direct) and q (quadratic) axis components, if available, to diagnosis purposes [5,6]. Other authors consider the rotor flux components and the current error signals while the stator torque current is proposed as a diagnostic index [6,7].

The field-oriented control (FOC) approach is presented in [7,8], and applied for the diagnosis of machines with broken rotor bars in closed loop (Park model) [9–12]. So, in this paper, it has been used for reduced model of induction machine in cases of none and faulted modes.

Fault detection has been already largely investigated, and different techniques applied for motor. Some methods utilized to detect motor failures, such as chromatographic analysis, noise analysis, temperature analysis and vibration analysis, have been slowly changing to new on-line monitoring techniques for electrical equipments [13–15]. Vibration monitoring techniques are usually installed on expensive and sensitive machines, where the cost of such systems can be justified. Moreover, the environmental sensitivity of the sensors can provide unreliable indications. Other approaches are based on the spectrum analysis; the advantage of this technique is that it is well recognized nowadays as a standard

* Corresponding author at: LGEB Laboratory, University of Biskra, Algeria.
E-mail address: h_Talhaoui@yahoo.fr (H. Talhaoui).

http://dx.doi.org/10.1016/j.isatra.2014.06.003
0019-0578/

Nomenclature

V_{DC}	DC bus voltage
V_a, V_b, V_c	instantaneous voltage a, b, c components
V_α, V_β	instantaneous voltage α, β components (Clarke)
V_d, V_q	instantaneous voltage d, q components (Park)
i_a, i_b, i_c	instantaneous current a, b, c components
i_α, i_β	instantaneous current α, β components (Clarke)
i_d, i_q	instantaneous current d, q components (Park)
V_{dsref}, V_{qsref}	d-axis voltage and q-axis voltage references (stator)
i_{dsref}, i_{qsref}	d-axis current and q-axis current references (stator)
I_{bk}	current of the bar k
I_{rk}	rotor current of mesh k
I_e	current in the ring of short circuit
I_{ek}	current in a portion of ring k
$[I]$	motor-current vector
$[L]$	motor-inductance matrix
$[R]$	motor-resistance matrix
$[V]$	motor-voltage vector
s	motor slip
K	integer
α	angle position between two broken bars
θ	angle between stator phase 1 and od axis
ω_r	electrical speed of the rotor in rad/s
C_e, C_r	electromagnetic and load torques
μ_0	Magnetic permeability of the air
mmf	magneto motive force

due to its simplicity: it needs only one current sensor per machine and is based on straightforward signal processing techniques such as fast Fourier transforms (FFT). However, it has mainly been designed for fixed frequency supply, such as for machines connected to the electrical grid (steady-state) [3,10]. Fault diagnosis in a closed-loop drive presents difficulties that are not presented when a constant 50/60 Hz power supply or an open-loop drive (motor is also supplied by a voltage source) are considered [12]. Some authors have addressed this problem using soft computing techniques or extensions of the motor current signature analysis (MCSA) method (requiring the analysis of the input electrical quantities spectrum) [3,15]. The major shortcomings of MCSA are its dependency on the motor speed and load; it does not always achieve good results when the speed or the load torque are not constant, which leads a variation on the motor slip (non-stationary signal); the fast Fourier transform cannot be used [16]. The solution is based on using the wavelet decompositions, which constitutes an alternative approach that avoids some problems encountered with the traditional method. The main goal of this paper is to proposition of a new method based on the discrete wavelet transform.

Wavelet transform is an analysis method for time-varying or non-stationary signals and uses a description of spectral decomposition via the scaling concept. Wavelet theory provides a unified framework for a number of techniques, which have been developed for various signal-processing applications [17]. One of its features is multi-resolution signal analysis with a vigorous function of both time and frequency localization. This method is effective for stationary as well as non-stationary signal processing. References [18,19] describe the pyramidal algorithm based on convolutions with quadrature mirror filters, which is a fast method (similar to the fast Fourier transform for signal decomposition and reconstruction), It can be interpreted as a decomposition of original signal in an orthonormal wavelet basis or as a decomposition of signal into a set of independent frequency bands. This independence is due to the orthogonality of the wavelet functions [20].

In this paper, an analysis of induction motor fault for closed loop using sensorless field oriented control is presented. The rotor speed is estimated by Luenberger observer. In this context, the main aim for this paper is to present a new method based on stator torque current and stator-current analysis for online fault detection in case of induction motors, which would overcome the averaging problems of classical FFT. Also, the proposed solution is based on analysis by wavelet decompositions. Simulation results are given for illustration.

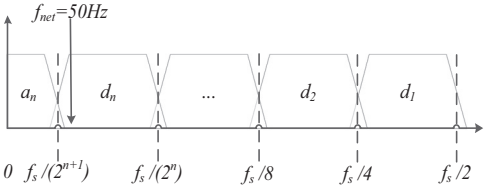

Fig. 1. Filtering process performed by the DWT.

2. Discrete wavelet transforms (DWT)

The wavelet transform is a time–frequency analysis technique. It decomposes a signal in terms of oscillations (wavelets) in both time and frequency. Its main idea is the dyadic bandpass filtering process carried out by this transform. Given a certain sampled signal $S=(S_1, S_2 \ldots S_n)$, the DWT decomposes it into several wavelet signals an approximation signal a_n, and n detail signals d_j ($j \in [1,n]$) [21,22]. The frequencies of approximation and detail signals can be given by

$$f(d_j) \in [2^{-(j+1)}f_s, 2^{-j}f_s] \quad (1)$$

$$f(a_n) \in \left[0, 2^{-(n+1)}f_s\right] \quad (2)$$

More concretely, f_s (samples/s): the sampling rate used for capturing S, the detail signal d_j contains the information concerning the signal components with frequencies included in the interval.

Therefore, the DWT carries out the filtering process shown in Fig. 1. Note that the filtering is not ideal, a fact leading to a certain overlap between adjacent frequency bands. This causes some distortions if a certain frequency component of the signal is close to the limit of band.

Due to the automatic filtering performed by the wavelet transform, the tool provides a very attractive flexibility for the simultaneous analysis of the transient evolution of rather different frequency components present in the same signal.

In comparison with other tools, the computational requirements are low. In addition, the DWT is available in standard commercial software packages. So no special or complex algorithm is required.

3. Modeling of induction motor rotor fault

In this study, the start-up transient current signature is selected for detection and diagnosing of faults in an induction motor. This method is effective because the machine is subjected to more stresses during the start-up above those of normal operation. These stresses can highlight the machine defects, those are early in

Please cite this article as: Talhaoui H, et al. Fast Fourier and discrete wavelet transforms applied to sensorless vector control induction motor for rotor bar faults diagnosis. ISA Transactions (2014), http://dx.doi.org/10.1016/j.isatra.2014.06.003

their development and not detected easily during steady state operation.

Fig. 2 describes the steps that should be followed in order to apply the DWT based methodology for the diagnosis of rotor faults (broken rotor bars).

To improve the effectiveness of the diagnostic procedure, it is useful to obtain further information on the health state of the machine. For this purpose, a transient model of the healthy machine is required. To develop our model, we have taken into account the effective geometry of the rotor that considers the rotor squirrel cage as a system of (N_r+1) identical and equally spaced loops, where N_r is the number of rotor bars as illustrated in Fig. 3.

In order to make the analysis easier, several assumptions are made as follows [23]:

- negligible saturation and skin effect;
- uniform air-gap;
- sinusoidal magneto motive force (mmf) of stator windings in air-gap;
- rotor bars are insulated from the rotor, thus no inter-bar current flows through the laminations; and
- relative permeability of machine armatures is assumed infinite.

Although the mmf of the stator windings is supposed to be sinusoidal, other distributions of rolling up could also be considered by simply employing the superposition theorem. It is justified by the fact that the different components of the space harmonics do not act the ones on the others.

Of course, the calculation of all the machine inductances is the key to the successful simulation of an induction machine. These inductances are conveniently computed by means of an analytical approach. Generally, this approach is based on the inductance concept, which is based on a linear flux–current relation.

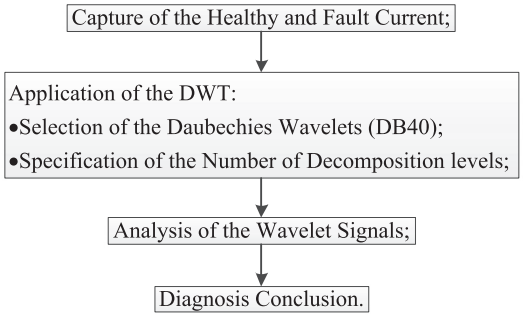

Fig. 2. Flowchart for the DWT-based diagnosis methodology.

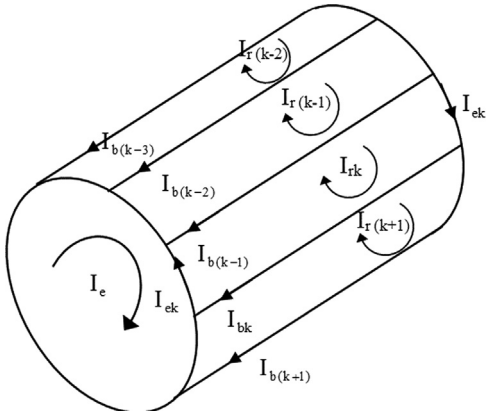

Fig. 3. Rotor cage equivalent circuit.

3.1. Stator inductance

The expression of mmf a phase "*a*" is given by the following:

$$F(\theta)=\frac{2N_s}{\pi.p}i_{as}\ \cos\ \theta \tag{3}$$

The induction created in the air-gap can be written as

$$B(\theta)=\frac{2}{\pi}\mu_0\frac{N_s}{e.p}i_{as}\ \cos\ p\theta \tag{4}$$

The main flux is thus written as

$$\phi_s=\frac{4}{\pi}\mu_0\frac{N_s^2}{e.p^2}R.l.i_{as} \tag{5}$$

The principal inductance of the magnetizing stator phase is

$$L_{sp}=4\mu_0\frac{N_s^2R.l}{e.p^2\pi} \tag{6}$$

Therefore the total inductance of a phase is equal to the sum of the magnetizing and leakage inductances, thus

$$L_{as}=L_{sp}+L_{sf} \tag{7}$$

The mutual inductance between the stator phases is computed as

$$M_s=-\frac{L_s}{2}. \tag{8}$$

3.2. Rotor inductance

The form of the magnetic induction produced by a rotor mesh in the air-gap is supposed to be radial and is represented in Fig. 4. The principal inductance of a rotor mesh can be calculated from the magnetic induction distribution shown in Fig. 4 [5,24]

$$L_{rp}=\left(\frac{N_r-1}{N_r^2}\right)\frac{\mu_0}{e}2\pi.R.l \tag{9}$$

The total inductance of the *k*th rotor mesh is equal to the sum of its principal inductance, inductance of leakage of the two bars and inductance of the leakage of the two portions of the rings of the short circuit closing the mesh *k* as indicated in Fig. 3.

$$L_{rr}=L_{rp}+2L_b+2L_e \tag{10}$$

$$M_{rr}=-\frac{1}{N_r{}^2}\frac{\mu_0}{e}2\pi.R.l \tag{11}$$

The *k*th mutual inductance between the adjacent meshes is given by

$$M_{rk(k-1)}=M_{rk(k+1)}=M_{rr}-L_b \tag{12}$$

The expression for the mutual inductance stator–rotor is can be calculated using the flux and is given by

$$M_{snrk}=-M_{sr}\ \cos\left(p\theta_r-n\frac{2\pi}{3}+k.\alpha\right) \tag{13}$$

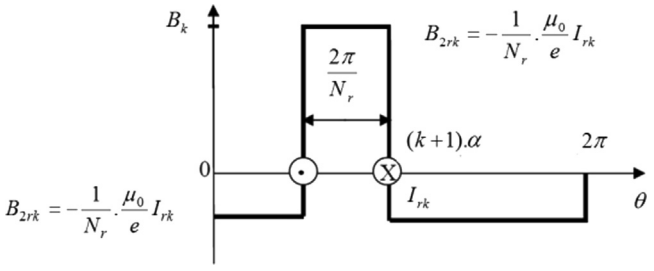

Fig. 4. Form of magnetic induction of rotor mesh created by two bars.

Please cite this article as: Talhaoui H, et al. Fast Fourier and discrete wavelet transforms applied to sensorless vector control induction motor for rotor bar faults diagnosis. ISA Transactions (2014), http://dx.doi.org/10.1016/j.isatra.2014.06.003

where $\alpha = p(2\pi/N_r)$ is the electrical angle of two adjacent rotor meshes, and $M_{sr} = (4/\pi)(\mu_0/e.p^2)N_s R.l \sin(\alpha/2)$.

The representation of the state is apparently a system of very high order. The application of transformation the Park's extended of rotor system so as to transform the system in N_r phases in a system (d, q).

A model of the reduced size of induction motor is obtained. The system in canonical form

$$[L]\frac{d[I]}{dt} = [V] - [R][I] \tag{14}$$

where

$$[L] = \begin{bmatrix} L_{sc} & 0 & -\frac{N_r}{2}M_{sr} & 0 & 0 \\ 0 & L_{sc} & 0 & -\frac{N_r}{2}M_{sr} & 0 \\ -\frac{3}{2}M_{sr} & 0 & L_{rc} & 0 & 0 \\ 0 & -\frac{3}{2}M_{sr} & 0 & L_{rc} & 0 \\ 0 & 0 & 0 & 0 & L_e \end{bmatrix},$$

$$[R] = \begin{bmatrix} R_s & -\omega L_{sc} & 0 & \frac{N_r}{2}\omega M_{sr} & 0 \\ \omega L_{sc} & R_s & -\frac{N_r}{2}\omega M_{sr} & 0 & 0 \\ 0 & 0 & [R_{rdd} & R_{rdq}] & 0 \\ 0 & 0 & [R_{rqd} & R_{rqq}] & 0 \\ 0 & 0 & 0 & 0 & R_e \end{bmatrix}$$

with $L_{rc} = L_{rp} - M_{rr} + 2(L_e/N_r) + 2L_e(1 - \cos\alpha)$.

The four terms are

$$\begin{cases} R_{rdd,rqq} = R_r + \frac{2}{N_r}(1 - \cos\alpha)\sum_k R_{bfk}(1 \pm \cos(2k-1)\alpha) \\ R_{rdq,rqd} = -\frac{2}{N_r}(1 - \cos\alpha)\sum_k R_{bfk} \sin(2k-1)\alpha \end{cases}. \tag{15}$$

In this expression, the summation is applied to all bars with fault. R_{bfk} is the increased resistance of the bar index k from its initial value before the fault.

The expression of the torque is given by

$$C_e = \frac{3}{2}PN_r.M_{sr}(i_{ds}.i_{qr} - i_{qs}.i_{dr}) \tag{16}$$

The model considered allows studying the behavior at the healthy and faulty state of the machine in different operation cases.

4. Field oriented control

The principle of field oriented control (FOC) is that the d–q coordinate's reference frame is locked to the rotor flux vector, thus, $\phi_{qr} = 0$, this results in a decoupling of the variables so that flux and torque can be separately controlled by the stator direct axis current i_{ds}, and quadrature-axis current i_{qs}, respectively, like in the separately excited dc machine.

The electromagnetic torque with the expression [7,8]

$$C_e = p\frac{3}{2}\frac{M}{L_{rc}}(\phi_{dr}i_{qs} - \phi_{qr}i_{ds}) \tag{17}$$

where $M = -(N_r/2).M_{sr}$The rotor flux components expressed in the stator reference frame

$$\begin{cases} \phi_{ds} = L_{sc}.i_{ds} - \frac{N_r}{2}M_{sr}.i_{dr} \\ \phi_{qs} = L_{sc}.i_{qs} - \frac{N_r}{2}M_{sr}.i_{qr} \\ \phi_{dr} = -\frac{3}{2}M_{sr}.i_{ds} + L_{rc}.i_{dr} \\ \phi_{qr} = -\frac{3}{2}M_{sr}.i_{qs} + L_{rc}.i_{qr} \end{cases}$$

To achieve field orientation along the rotor flux, the direct flux component is aligned in the direction of rotor flux ϕ_r. At this condition

$$\begin{cases} \phi_{dr} = \phi_r \\ \phi_{qr} = 0 \end{cases} \tag{18}$$

Hence the equations ensuring the field orientation are expressed as

$$\begin{cases} i_{ds} = \frac{1+T_r.S}{M_r}\phi_{dr} \\ i_{qs} = \frac{C_e}{K_t\phi_{dr}} \end{cases} \tag{19}$$

$M_r = -(3/2).M_{sr}$, S: Laplace operator, and $T_r = L_{rc}/R_r$: rotor time constant.

Under these conditions, the induction machine is transformed into a linear current/torque converter

$$C_e = p\frac{3}{2}.\frac{M}{L_{rc}}\phi_{dr}i_{qs} = k_t.\phi_{dr}.i_{qs} \tag{20}$$

Fig. 5 illustrates the block diagram of FOC scheme using Luenberger observer for speed estimation and the loop control using PI regulator. The rotor speed ω_r is compared with the reference speed ω_{ref} and adjusted by the PI controller. The output

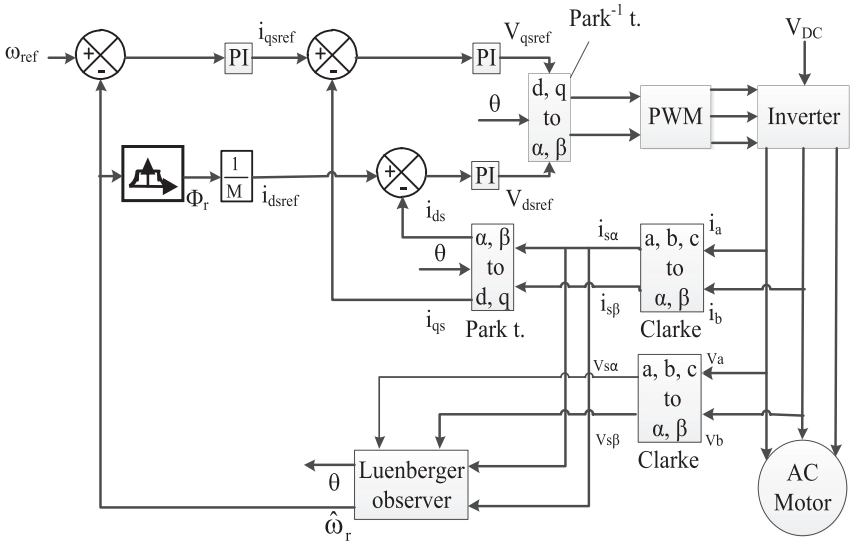

Fig. 5. Basic scheme of FOC for AC-motor.

Please cite this article as: Talhaoui H, et al. Fast Fourier and discrete wavelet transforms applied to sensorless vector control induction motor for rotor bar faults diagnosis. ISA Transactions (2014), http://dx.doi.org/10.1016/j.isatra.2014.06.003

of this is considered to be the reference quadratic current i_{qsref}. In the look-up table used for field-weakening, the flux is assumed to be constant when the motor operates below the rated speed and beyond the rated speed, the flux speed product is held constant [9,25].

Two-phase currents are measured. These measurements feed the Clark transformation module. The outputs of this projection are designated $i_{s\alpha}$ and $i_{s\beta}$. These current components are the inputs of the Park transformation that gives the current in the (d, q) rotating reference frame. The i_{ds} and i_{qs} components are compared to the references i_{dsref} (the flux reference) and i_{qsref} (the torque reference). As induction motors need a rotor flux creation in order to operate, the flux reference must not be zero. The torque command i_{qsref} could be the output of the speed regulator when we use a speed FOC. The outputs of the current regulators are V_{dsref} and V_{qsref}; they are applied to the inverse Park transformation. The outputs of this projection are $V_{s\alpha ref}$ and $V_{s\beta ref}$, which are the components of the stator vector voltage in the (α, β) stationary orthogonal reference frame. These are the inputs of the Space Vector PWM.

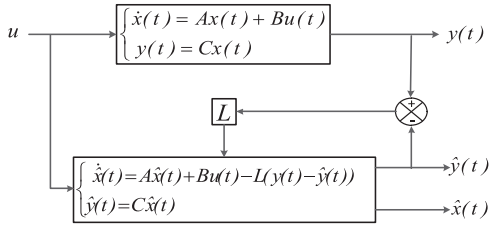

Fig. 6. Principle of the observer diagrams.

5. Sensorless speed control algorithm

The state model of the induction motor can be described in a rotating reference frame by

$$\begin{cases} \dot{x}(t) = Ax(t) + Bu(t) \\ y(t) = Cx(t) \end{cases} \tag{21}$$

The Luenberger state observer for estimating the stator current and the rotor flux, using the measured stator currents and voltages,

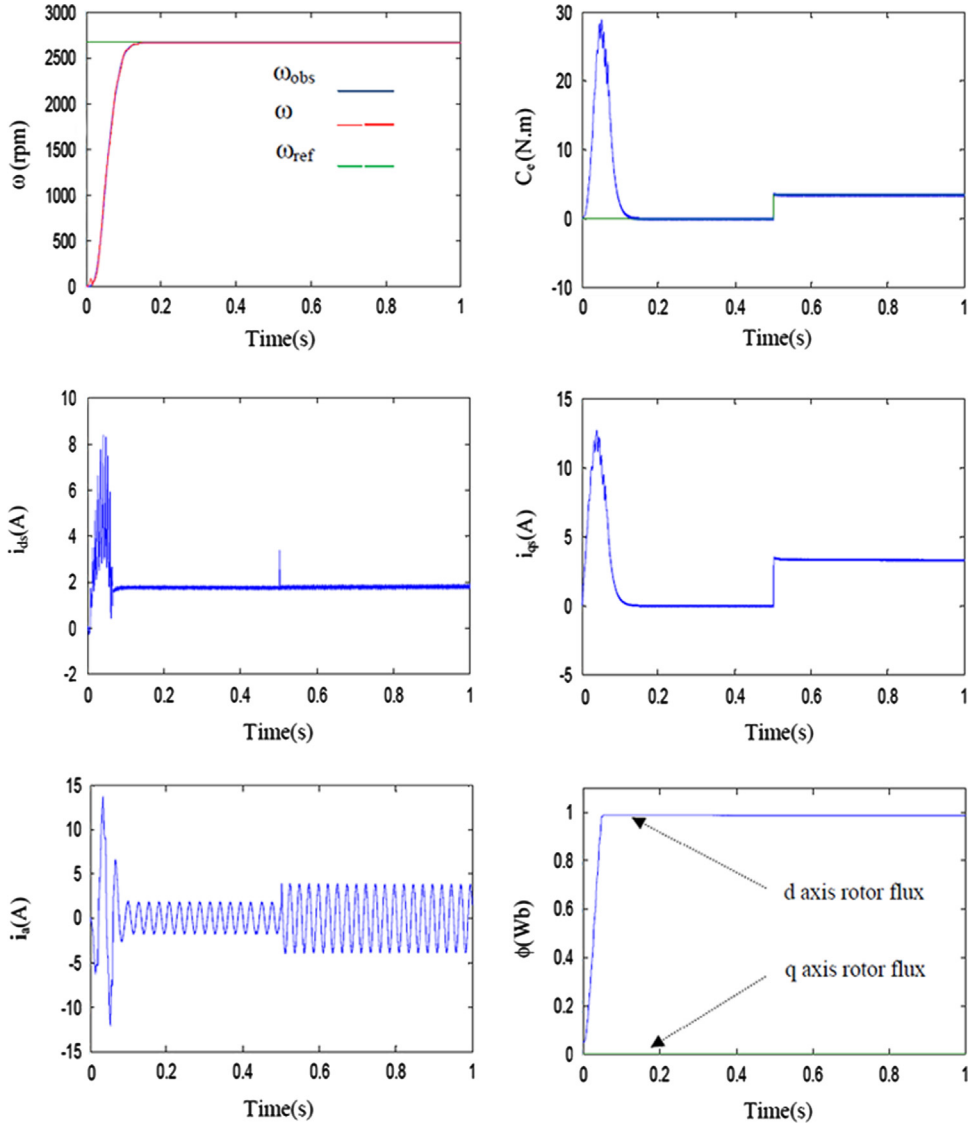

Fig. 7. Simulation results for vector control of induction motor.

Please cite this article as: Talhaoui H, et al. Fast Fourier and discrete wavelet transforms applied to sensorless vector control induction motor for rotor bar faults diagnosis. ISA Transactions (2014), http://dx.doi.org/10.1016/j.isatra.2014.06.003

is described by the following set of equations [26]:

$$\begin{cases} \dot{\hat{x}}(t) = (A - LC)\hat{x}(t) + Bu(t) + L\hat{y}(t) \\ \hat{y}(t) = C\hat{x}(t) \end{cases}$$

$$[x] = \begin{bmatrix} i_{s\alpha} & i_{s\beta} & \phi_{r\alpha} & \phi_{r\beta} \end{bmatrix},\ [\hat{x}] = \begin{bmatrix} \hat{i}_{s\alpha} & \hat{i}_{s\beta} & \hat{\phi}_{r\alpha} & \hat{\phi}_{r\beta} \end{bmatrix} \quad (22)$$

$$[y] = \begin{bmatrix} i_{s\alpha} & i_{s\beta} \end{bmatrix}^T, [\hat{y}] = \begin{bmatrix} \hat{i}_{s\alpha} & \hat{i}_{s\beta} \end{bmatrix}^T,\ [u] = \begin{bmatrix} V_{s\alpha}, V_{s\beta} \end{bmatrix}^T$$

where ^ denotes the estimated values, $\hat{x}(t)$ is the observer state vector and L is the observer gain matrix, which is selected so that the system will be stable (Fig. 6).

To ensure that the estimation error vanish over time for any, $\hat{x}(0)$ we should select the observer gain matrix L so that (A-LC) is asymptotically stable. Therefore, the observer gain matrix should be chosen so that all Eigen values of (A-LC) have negative real parts [27]. The adaptive scheme for speed estimation is given by

$$\hat{\omega}_r = k_p(e_{is\alpha}.\phi_{r\beta} - e_{isb}.\phi_{r\alpha}) + k_i \int (e_{is\alpha}.\phi_{r\beta} - e_{isb}.\phi_{r\alpha})dt \quad (23)$$

where $e = x - \hat{x}$, k_p and k_i are respectively the proportional and integral constants.

6. Simulation results

The simulations of the sensorless field oriented control (FOC) induction motor drive were carried out using the Matlab/Simulink (Runge–Kutta, order 4) simulation package. The motor used in the simulation study is a 1.1 kW, 220 V, 50 Hz, 2-pole induction motor, with a rotor with 16 bars. The system parameters of the induction motor tested in this study are given in Appendix A.

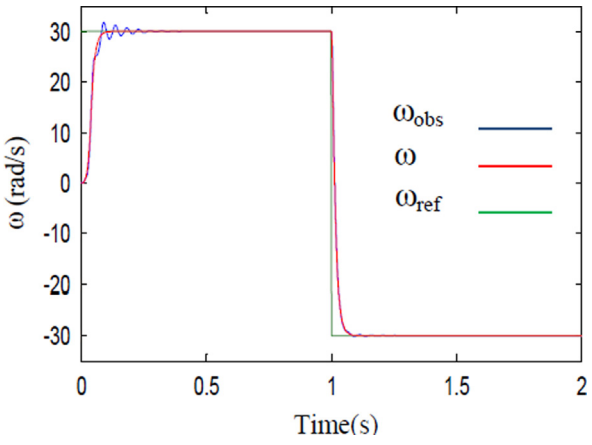

Fig. 8. Reverse low speed test.

6.1. Results for vector control of induction motor

To illustrate the performances of the control, a simulation with reference speed equal to 2670 rpm is realized (Fig. 7), a nominal load=3.5 N m is applied at t=0.5 s.

The estimated speed tracks the real speed with no steady-state error; the torque and stator phase current have a very good dynamic. Quadratic rotor flux ϕ_{qr} is maintained to almost zero, ϕ_{dr} is stabilized to its rated value. The obtained results are successful, and they validate the proposed scheme.

Fig. 7 shows that the performance of the vector control of the induction motor drive is exactly the same as the performance of the separately excited DC motor.

Fig. 8 illustrates the time response of the rotating speed. The reverse test of speed is realised by changing the speed reference from 30 rad/s to −30 rad/s at t=1 s.

Fig.8 shows the good performance of the sensorless vector control, when the induction motor operates at low reference speed. It shows that the errors of estimate rotor speed observer and the real rotor speed is very less.

6.2. Results for healthy machine

Fig. 9 shows the speed, the stator current and the quadratic current of control under healthy conditions of the machine, the test of control is realised with reference speed equal 2670 rpm and with nominal load apply at the start up.

6.3. Results for machine with fault

To highlight the effect of the break severity, we simulate bars break by increasing the broken bar resistance Eq. (15). In this case, the machine operates initially with nominal load and fault: two broken rotor bar (Fig. 10).

From Figs. 9 and 10, currents for the healthy and faulty state of the machine have a little difference, and their torque control currents have significant difference. In this case, the speed gives no information about the presence of fault due to the rotors speed pulsation is compensated by the control of the system.

6.4. FFT analysis

In order to analyze the harmonics frequency bring about the broken rotor bar fault, the spectrum analysis by FFT is used for the stator currents, the speed and quadratic current of control. Several quantities were calculated and analyzed in control to access the information they contained about the presence of the simulated fault (two broken rotor bars).

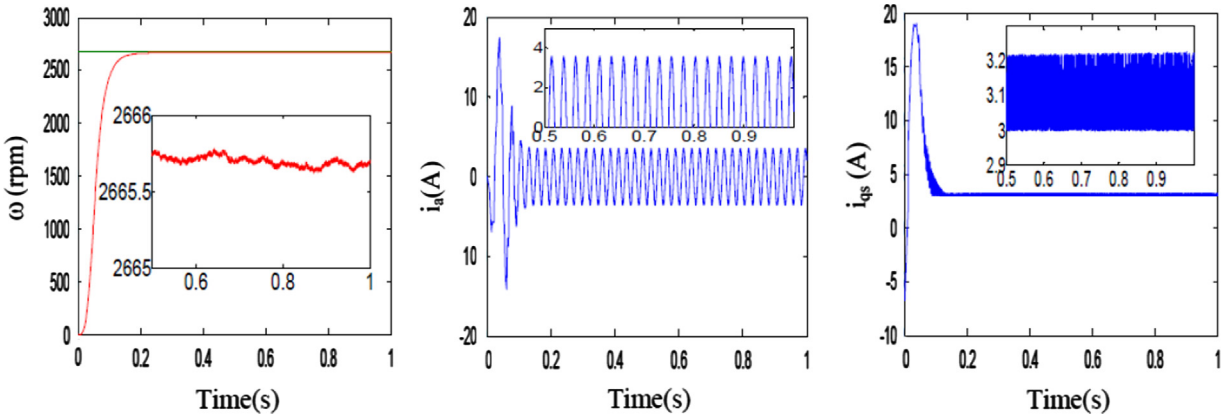

Fig. 9. Speed, stator current and quadratic current i_{qs} for the healthy state.

Please cite this article as: Talhaoui H, et al. Fast Fourier and discrete wavelet transforms applied to sensorless vector control induction motor for rotor bar faults diagnosis. ISA Transactions (2014), http://dx.doi.org/10.1016/j.isatra.2014.06.003

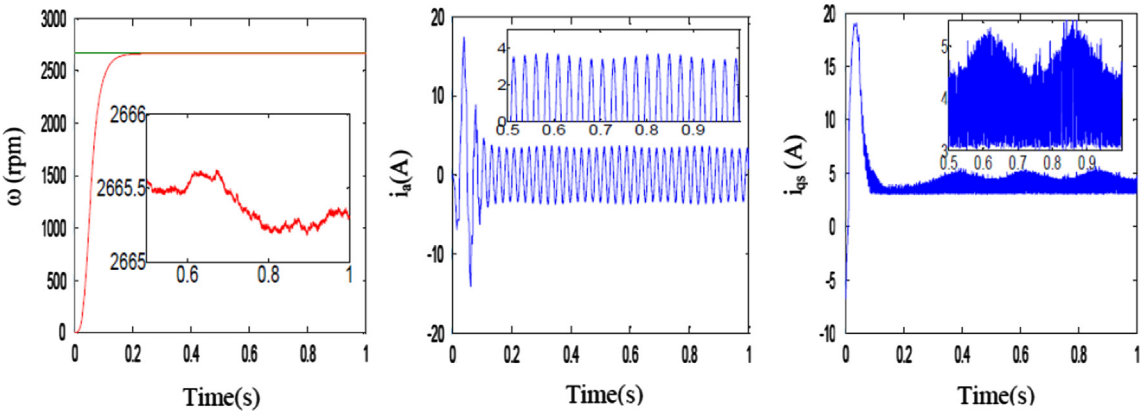

Fig. 10. Speed, stator current and quadratic current i_{qs} for the faulty state: two rotor broken bar.

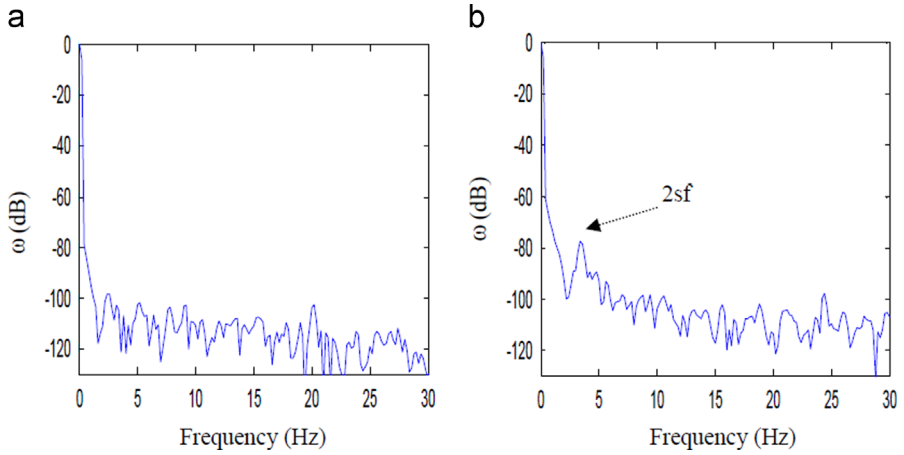

Fig. 11. Speed spectrum in steady state: (a) healthy state and (b) faulty state: two broken rotor bars (1 and 2).

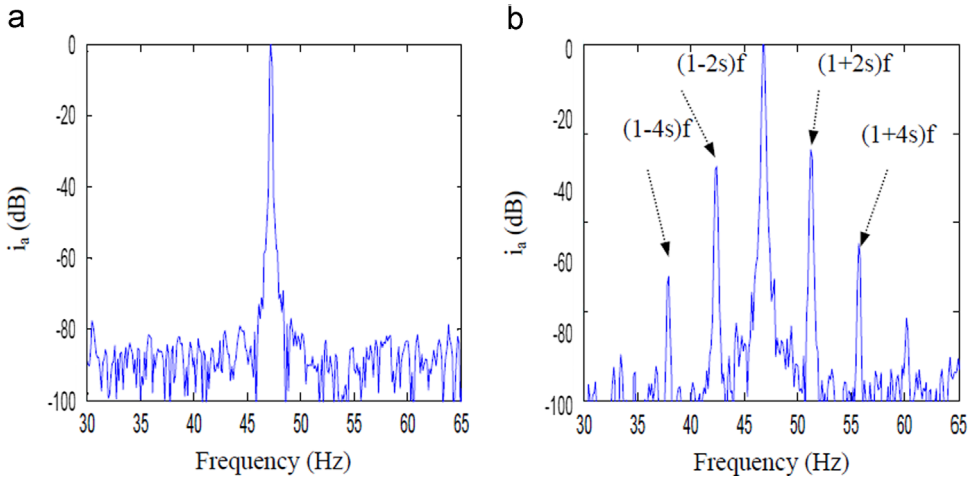

Fig. 12. FFT of stator current in steady state: (a) healthy state and (b) faulty state: two broken rotor bars.

Fig. 11 shows the spectrum for the speed of induction motor at full load at healthy and faulty sate (the reference speed 2670 rpm, 44.5 Hz).

Identification of fault presence by spectrum analysis of speed (Fig. 11) is very difficult owing to control loop action. Fig. 12 illustrates the result of frequency analysis of the stator current.

The spectral analysis of the stator currents highlights the effect of the defect through the appearance of harmonics around the fundamental [5]. Their magnitudes increase according to the number of defective bars at characteristic frequencies Eq. (24), [10]

$$f_{defect} = (1 \pm 2Ks)f \tag{24}$$

where $K = 1, 2, 3, \ldots$,f is the frequency training of the machine and s is the fractional slip of the motor.

It is also noted that the calculated frequencies are very near from the deduced ones in the simulation (Table 1).

Please cite this article as: Talhaoui H, et al. Fast Fourier and discrete wavelet transforms applied to sensorless vector control induction motor for rotor bar faults diagnosis. ISA Transactions (2014), http://dx.doi.org/10.1016/j.isatra.2014.06.003

Table 1
Magnitude and frequencies of the stator current spectrum for the machine with two broken rotor bars.

s=4.853%	$(1-4s)f$	$(1-2s)f$	$(1+2s)f$	$(1+4s)f$
$f_{calculated}$ (Hz)	37.691	42.2305	51.3094	55.8489
$f_{deduced}$ (Hz)	37.83	42.27	51.31	55.73
Magnitude (dB)	−52.5	−26.67	−23.62	−44.82

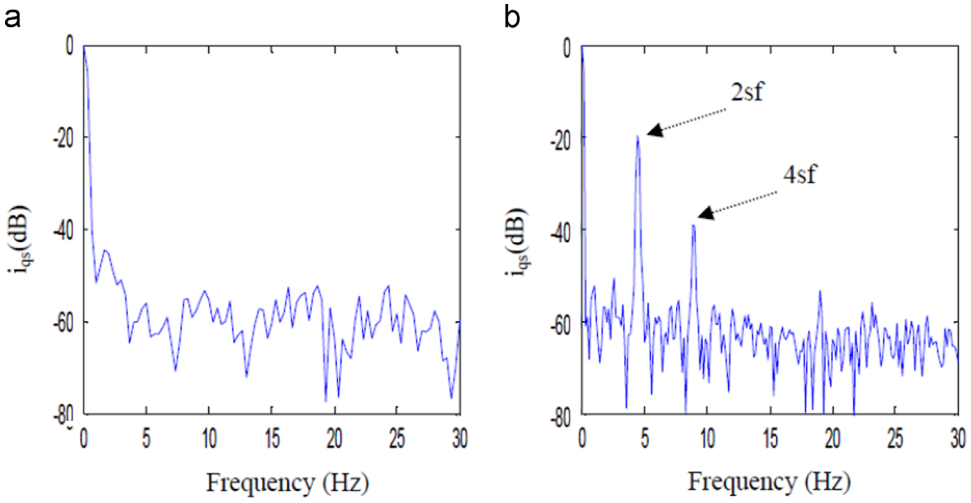

Fig. 13. Spectrum of i_{qs} in steady state: (a) healthy state and (b) faulty state: two broken rotor bar.

Table 2
Magnitude and frequencies of quadratic current i_{qs} spectrum for the machine with two broken rotor bars.

s=4.853%	$2sf$	$4sf$
$f_{calculated}$ (Hz)	4.5394	9.0789
$f_{deduced}$ (Hz)	4.449	8.96
Magnitude (dB)	−20.67	−40.1

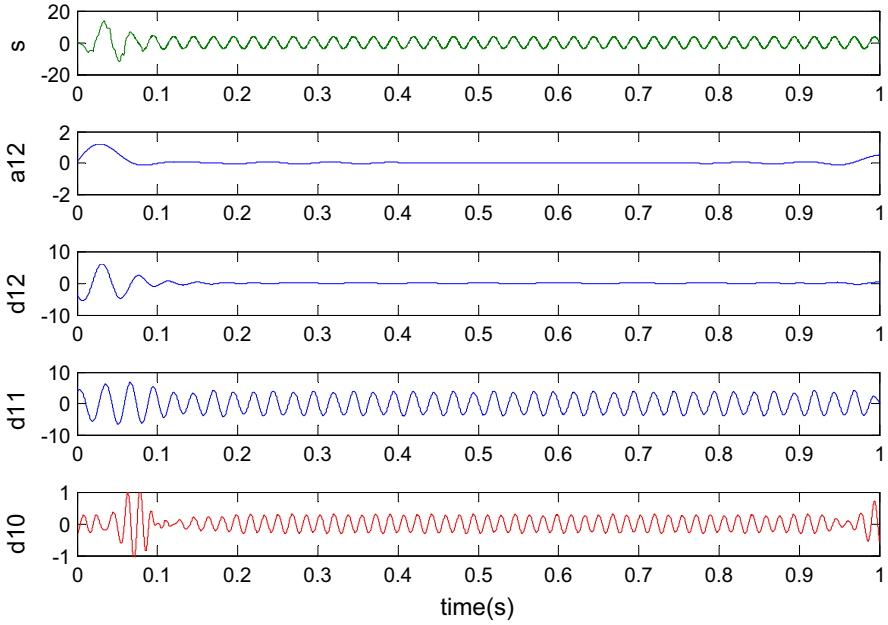

Fig. 14. DWT analysis of current stator at startup operate state and at full load for the healthy machine.

Please cite this article as: Talhaoui H, et al. Fast Fourier and discrete wavelet transforms applied to sensorless vector control induction motor for rotor bar faults diagnosis. ISA Transactions (2014), http://dx.doi.org/10.1016/j.isatra.2014.06.003

If the machine operates with fault, the rotor speed pulsation is compensated by the control system. It is noted, that the component control of torque i_{qs} has an appropriate characteristic for the diagnostic fault.

The harmonics component for the i_{qs} current appear at $2sf$ (Fig. 13), So, the magnitude of these harmonics is affected by the speed loop gain. Table 2 shows that the values of deduced and calculated frequencies are similar.

In Figs. 13 and 14, the result of rotor broken bars sees an increase in the magnitude of harmonics amplitude of the stator current and quadratic current.

Simulation results show the impact and the effectiveness of failure. Tests are validated by numerical simulation, and the obtained results show clearly the possibility of extracting signatures to detect and locate the faults.

The FFT transform is an effective method and widely used in signal processing; the signal may lose some time-domain information. The limitation of FFT appears in the non-stationary signals lead to the introduction of time–frequency or time scale signal processing tools, assuming the independence of each frequency channel when the original signal is decomposed. This assumption may be considered as the limitation of this approach [23]. The solution based is an analysis by wavelet decompositions.

6.5. DWT analysis

The decomposition level n depends on the sampling rate f_s and on the frequency net f_{net} and can be calculated using by [5,19]

$$n > \frac{\log(f_s/f_{net})}{\log(2)} + 1 \tag{25}$$

The sampling rate of signals was $f_s = 100{,}000$ samples/s. The supply frequency in this paper is taken to be $f_{net} = 50$ Hz. Table 3 shows the frequency band for each level.

Fig. 14 shows the DWT of the stator current at startup sate given in Fig. 9, Daubechies wavelets of different order are used to decompose the signal. The approximation and detail signals obtained from stator currents by 40 db in the healthy state are a12, d12, d11 and d10.

The same DWT decomposition more precisely at a12, d12, d11 and d10 signals in the case the machine with two broken rotor bars (Fig. 15)

Extracted information fundamental has a very significant effect on the diagnosis; the effect is interpreted by magnitude signal increasing in bands d10, in the case of a machine with fault (Fig. 15).

Although there are differences of the detail coefficients for the failed motor, it is not convenient to directly compare both of them, since at these levels the fundamental component (50 Hz) plays an important role, and it is present in the whole analysis. Due to the above inconvenience, quadratic current i_{qs}, to eliminate the fundamental component in both signals.

Figs. 16 and 17 show respectively the DWT of quadratic current i_{qs} for the machine with healthy and faulty sate: two broken rotor bars.

In Figs. 16 and 17, the analysis of the signals resulting from the wavelet decomposition shows a particular variation in the d10 level only, which fits the characteristic pattern mentioned before, caused by the fault (broken rotor bars) in the machine. We could find important differences for the motor broken rotor bars since they contain the frequency components $2sf$, where give d10 all the information in the frequency band [48.82–97.65 Hz] (Table 3). From this, it can be affirmed that the method provides information about the presence of broken rotor bars in a loaded machine.

Table 3
Frequency levels of wavelet coefficients.

Level	Frequency band (Hz)
a12	0–12.20
d12	12.20–24.41
d11	24.41–48.82
d10	48.82–97.65

7. Conclusion

In this paper, methods of fault analysis of induction machine driven in close loop by sensorless field oriented control are presented. Two approach signals are used for broken rotor bar fault diagnosis, such as Fourier and DWT in stationary and non-stationary states for electric and mechanic components (stator current, speed and quadratic current). The Luenberger observer is

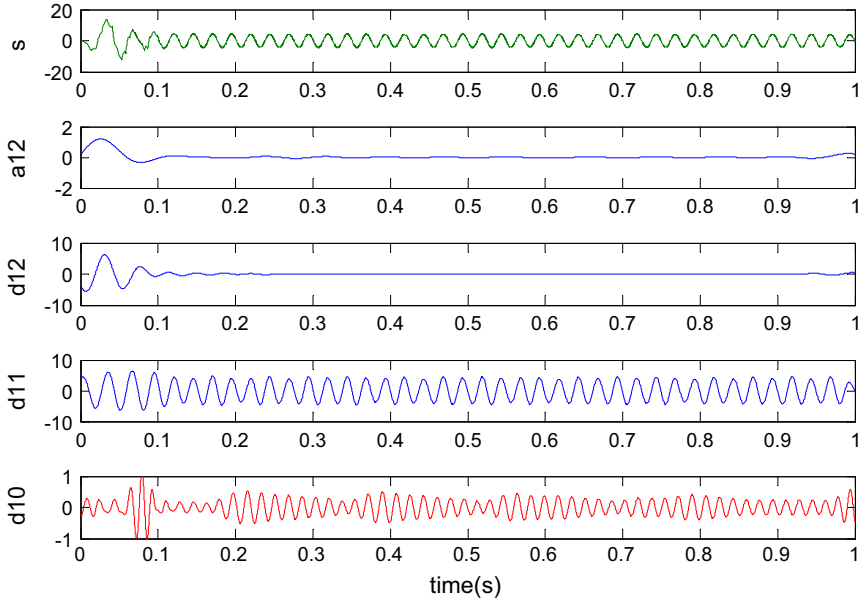

Fig. 15. DWT analysis of stator current (startup state with full load) for the faulty machine: 2 broken rotor bars.

Please cite this article as: Talhaoui H, et al. Fast Fourier and discrete wavelet transforms applied to sensorless vector control induction motor for rotor bar faults diagnosis. ISA Transactions (2014), http://dx.doi.org/10.1016/j.isatra.2014.06.003

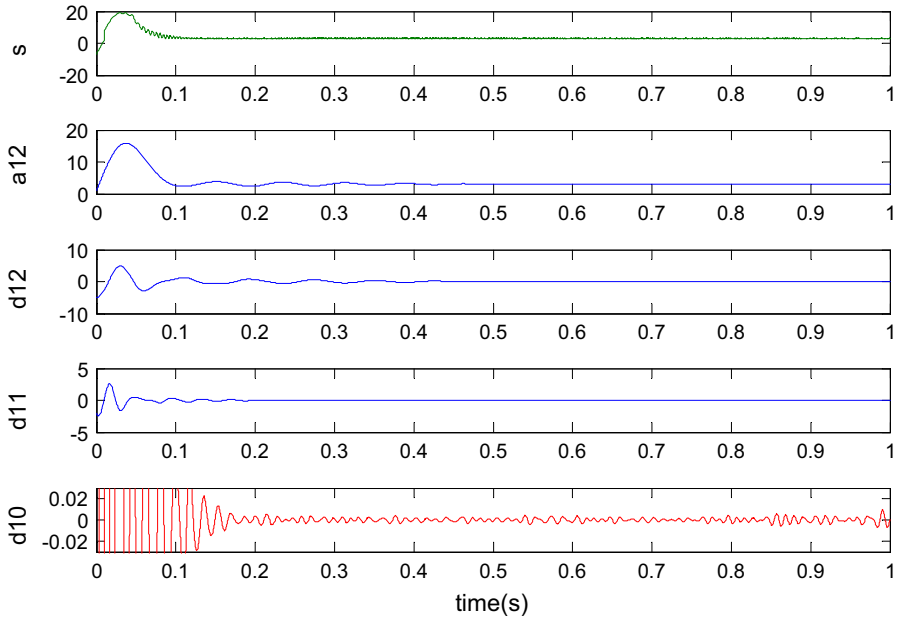

Fig. 16. DWT analysis of quadratic current i_{qs} at startup state and at full load for healthy machine.

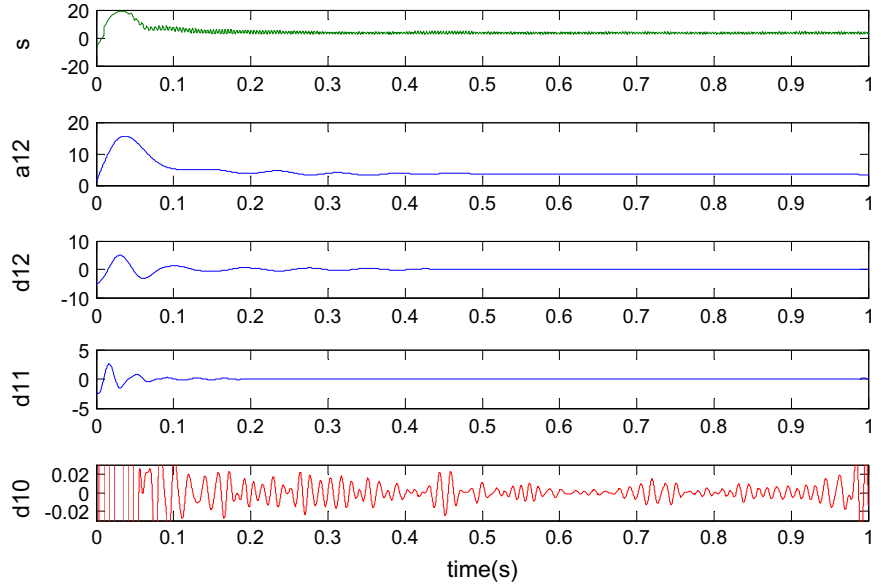

Fig. 17. DWT analysis of quadratic current i_{qs} at startup state and at full load for the faulty machine: 2 broken rotor bars.

used for estimate and analysis the rotor speed component (is very robust to all motor parameter changes, hence it should work properly in a faulty rotor). The effect of loop control by using the speed regulator ensures the rejection of ripples, thus the correlation with the faulty severity is lost. For this, the selection of internal signals of such control structure can be used as fault signatures for diagnostic purposes. The advantage of stator currents and quadratic current components' analysis offers a good sign for the rotor fault detection of the rotor fault. Obtained results by Fourier transform give good information from estimate frequencies values, sideband harmonics produced by the faulty part (broken rotor bar). This method has advantages in the steady state only. These techniques are not always insufficient to determine the fault degree; hence the complementary cooperation of DWT is required. Simulation results for this aim indicate that, the DWT method is a very effective and reliable technique for diagnosis. The failure can be detected during the motor operating, particularly in the case of broken rotor bars at a startup state.

Appendix A. For the simulated induction motor

P_n output power	1.1 kW
V_s stator voltage	220 V
f stator frequency	50 Hz
p pole number	1
R_s stator resistance	7.58 Ω
R_r rotor resistance	6.3 Ω
R_b rotor bar resistance	0.15 mΩ

Please cite this article as: Talhaoui H, et al. Fast Fourier and discrete wavelet transforms applied to sensorless vector control induction motor for rotor bar faults diagnosis. ISA Transactions (2014), http://dx.doi.org/10.1016/j.isatra.2014.06.003

R_e resistance of end ring segment	0.15 mΩ
L_b rotor bar inductance	0.1 μH
L_e inductance of end ring	0.1 μH
L_{sf} leakage inductance of stator	26.5 mH
M_{sr} mutual inductance	46.42 mH
N_s number of turns per stator phase	160
N_r number of rotor bars	16
L length of the rotor	65 mm
e air-gap mean diameter	2.5 mm
i inertia moment	0.0054 kg m^2

References

[1] Kar BN, Mohanty KB, Singh M. Indirect vector control of induction motor using fuzzy logic controller. In: Proceedings of IEEE 10th international conference of the environment and electrical engineering; 2011.
[2] Youn Y, Hwang D, Sun J, Kang D. A method for indentifying broken rotor bar and stator winding fault in a low-voltage squirrel-cage induction motor using radial flux sensor. J Electr Eng Technol 2011;6(5):666–70.
[3] Karamia F, Poshtan J, Poshtan M. Detection of broken rotor bars in induction motors using nonlinear Kalman filters. ISA Trans 2010;49:189–95.
[4] Ashari AE, Nikoukhah R, Campbell SL. Active robust fault detection in closed-loop systems: quadratic optimization approach. IEEE Trans Autom Control 2012;57(10).
[5] Saidi L, Fnaiech F, Henao H, Capolino G-A, Cirrincione G. Diagnosis of broken-bars fault in induction machines using higher order spectral analysis. ISA Trans 2013;52:140–8.
[6] Bellini A, Concari C, Franceschini G, Tassoni C. Different procedures for the diagnosis of rotor fault in closed loop induction motors drives. In: Proceedings of the IEEE electric machines & drives conference, IEMDC'07. Antalia; May 2007.
[7] Serna E, Pacas JM. Detection of rotor faults in field oriented controlled induction machines. In: Proceedings of the 41st IAS annual meeting, industry applications conference. Tampa; October 2006.
[8] Kamal MM, Yu D. Fault detection and isolation for PEMFC systems under closed-loop control. In: Proceedings of the UKACC international conference on control. Cardiff, UK; 3–5 September 2012.
[9] Orlowska-Kowalska T, Dybkowski M, Kowalski CT. Rotor fault analysis in the sensorless field oriented controlled induction motor drive. Automatika 2010;51(2):149–56.
[10] Kechida R, Menacer A, Benakcha A. Fault detection of broken rotor bars using stator current spectrum for the direct torque control induction motor. World Acad Sci, Eng Technol 2010;66.
[11] Talhaoui H, Menacer A, Kechida R. Rotor fault detection in sliding mode control induction motor using FFT and discrete wavelet transform. In: Proceedings of the 7th international conference on electrical engineering CEE'12. Batna, Algerie; October 08–10 2012.
[12] Toscani S, Faifer M, Rossi M, Cristaldi L, Lazzaroni M. Effects of the speed loop on the diagnosis of rotor faults in induction machines. IEEE Trans Instrum Meas 2012;61(10).
[13] Benbouzid M, Beguenane R, Viera M. Induction motor asymmetrical faults detection using advanced signal processing techniques. IEEE Trans Energy Convers 1999;14(2):146–52.
[14] Martelo A. Fault detection of ball bearing in electrical motors by means of vibration, noise and stator current spectral analysis [M.Sc. thesis]. Colombia: Department of Mechanical Engineering, University of Los Andes, Bogot´a; 2000 (in Spanish).
[15] Menacer A, Champenois G, Nait-Said MS, Benakcha A, Moreau S, Hassaine S. Rotor failures diagnosis of squirrel cage induction motors under different types of ac sources supplying. Electr Eng Technol (KIEE) 2009;4(2):219–28.
[16] Siddiqui KM, Giri VK. Broken rotor bar fault detection in induction motors using wavelet transform. In: Proceedings of the IEEE international conference on computing, electronics and electrical technologies; 2012.
[17] Gritli Y, Rossi C, Zarri L, Filippetti F, Chatti A, Casadei D. Double frequencyslid-ing and wavelet analysis for rotor fault diagnosis in induction motorsunder time-varying operating condition. In: Diagnostics for electric machines, power electronics & drives (SDEMPED), IEEE;2011. p. 676-83.
[18] Keskes H, Braham A, Lachiri Z. On the use of stationary wavelet packet transform and multiclass wavelet SVM for broken rotor bar detection. In: Proceedings of the IECON 2012–38th annual conference of IEEE Industrial Electronics Society; October 2012.
[19] Bouzida A, Touhami O, Ibtiouen R, Belouchrani A, Fadel M, Rezzoug A. Fault diagnosis in industrial induction machines through discrete wavelet trans-form. IEEE Trans Ind Electron 2011;58(9).
[20] Ibrahim MM, Nekad HJ. Broken bar fault detection based on the discrete wavelet transform and artificial neural network. Asian Trans Eng 2013;03(02) (ATE ISSN: 2221-4267).
[21] Kechida R, Menacer A, Talhaoui H. Approach signal for rotor fault detection in induction motors. J Fail Anal Prev 2013;13(3):346–52.
[22] Singh M, Yadav RK, Kumar R. Discrete wavelet transform based measurement of inner race defect width in taper roller bearing. Springer MAPAN – J Metrol Soc India 2013;28(1):17–23.
[23] Menacer A, Moreau S, Benakcha A, Nait Said MS. Effect of the position and the number of broken bars on asynchronous motor stator current spectrum. EPE – power electronics and motion control. Portoroz, Slovenia: Août; 2006.
[24] Kechida R, Menacer A, Benakcha A. Rotor's model taking account the faults for the direct torque control induction motor. In: Proceedings of the 18th Mediterranean conference on control and automation. Marrakech Morocco; June 23–25 2010.
[25] Rao P, Nakka J, Shekar R. Sensorless vector control of induction machine using MRAS techniques. In: Proceedings of the IEEE 2013 international conference on circuits, power and computing technologies [ICCPCT-2013].
[26] Trajin B, Regnier J, Faucher J. Detection of bearing faults in asynchronous motors using luenberger speed observer. In: Proceedings of the 34th Annual Conference of IEEE Industrial Electronics, IECON 2008.
[27] Rezgui SE, Benalla H. MRAS sensorless based control of IM combining sliding-mode, SVPWM, and Luenberger observer. In: Proceedings of the EUROCON – international conference on computer as a tool (EUROCON); 2011.

Please cite this article as: Talhaoui H, et al. Fast Fourier and discrete wavelet transforms applied to sensorless vector control induction motor for rotor bar faults diagnosis. ISA Transactions (2014), http://dx.doi.org/10.1016/j.isatra.2014.06.003